Northumbria Research Link

Citation: Che, Jian, Wang, Junsen, Qiao, Changcang, Xia, Yudong, Ou, Kai, Zhou, Jing, Ni, Yuxiang, Zhang, Wenting, Han, Yuchen, Zu, Xiaotao, Fu, Yong Qing and Tang, Yongliang (2023) Si-Cu nanocomposite as an effective sensing layer for H2S based on quartz surface acoustic wave sensors. Sensors and Actuators A: Physical, 353. p. 114225. ISSN 0924-4247

Published by: Elsevier

URL: https://doi.org/10.1016/j.sna.2023.114225 <https://doi.org/10.1016/j.sna.2023.114225>

This version was downloaded from Northumbria Research Link: https://nrl.northumbria.ac.uk/id/eprint/51346/

Northumbria University has developed Northumbria Research Link (NRL) to enable users to access the University's research output. Copyright © and moral rights for items on NRL are retained by the individual author(s) and/or other copyright owners. Single copies of full items can be reproduced, displayed or performed, and given to third parties in any format or medium for personal research or study, educational, or not-for-profit purposes without prior permission or charge, provided the authors, title and full bibliographic details are given, as well as a hyperlink and/or URL to the original metadata page. The content must not be changed in any way. Full items must not be sold commercially in any format or medium without formal permission of the copyright holder. The full policy is available online: http://nrl.northumbria.ac.uk/policies.html

This document may differ from the final, published version of the research and has been made available online in accordance with publisher policies. To read and/or cite from the published version of the research, please visit the publisher's website (a subscription may be required.)

Northumbria University NEWCASTLE

University Library

Si-Cu nanocomposite as an effective sensing layer for H_2S based on quartz surface acoustic wave sensors

Jian Che[a], Junsen Wang[a], Changcang Qiao[a], Yudong Xia[a], Kai Ou[a], Jing Zhou[a], Yuxiang Ni[a], Wenting Zhang[a], Yuchen Han[b], Xiaotao Zu[b], Yongqing Fu[c], Yongliang Tang[a,*]

[a]School of Physical Science and Technology, Southwest Jiaotong University, Chengdu, 610031, People's Republic of China

[b]School of Physics, University of Electronic Science and Technology of China, Chengdu, 610054, People's Republic of China

[c]Faculty of Engineering and Environment, Northumbria University, Newcastle upon Tyne, NE1 8ST, UK

*Correspondance to Yongliang Tang. Email: tyl@swjtu.edu.cn Tel:86-15884573263

ABSTRACT: It has been a critical challenge to develop highly sensitive H_2S gas sensors, due to its wide-range application in industry and frequent leakage, which endangers people's lives. In this work, a highly sensitive room-temperature SAW H_2S gas sensor based on Si-Cu nanocomposite was developed. The Cu content in this composite layer plays a key role for H_2S response of the sensor because CuO, an excellent adsorption site for H_2S, presents on the surface of Cu. The amorphous Si content results in the highly porous structure enhancing the interaction between CuO and H_2S. The interaction leads to the formation of CuS and a negative frequency response of the sensor. H_2O molecules effectively participate the reactions between CuO and H_2S, and the responses of H_2S were significantly enhanced in a moister environment. With the relative humidity of 60%, the sensor can detect 50 ppb H_2S with a response of -225 Hz.

Keywords: surface acoustic wave, gas sensor, H_2S, CuO, Si, humidity

1. Introduction

H_2S is highly toxic, and its toxicity is similar as that of cyanide and 5 times greater than that of CO [1-3]. It makes people feel uncomfortable at low concentration and can cause severe damage on nervous and respiratory systems, organs failure and death at relative high concentrations (>100 ppm) [4-6]. Nevertheless, H_2S is widely used in industrial production, especially in chemical, agriculture, and oil industries, which makes it becoming a serious threat for people's lives and property safety [7-11]. For example, on April 17, 2022, three people were killed with many injured in a hydrogen sulfide leakage incident in Yuyao, Zhejiang province, China. To prevent similar incidents, H_2S gas sensors with high sensitivity, selectivity and reliability are urgently needed for real time concentration surveillance.

Compared with traditional semiconductor and electrochemical gas sensors, surface acoustic wave (SAW) gas sensors based on piezoelectric effects are highly precise, sensitive, light, intelligent and wireless [12-14]. SAW gas sensor is composed of a radio frequency oscillator, which is generally made of a SAW resonator coated with a sensitive layer, along with its peripheral circuit [15]. When the gas-sensitive layer adsorbs the target gas molecules, the corresponding variations in mass, elastic modulus, electrical conductivity of this sensitive layer will have significant impact on wave velocity and resonant frequency of the SAW resonator [16], which results in apparent changes in the oscillating frequency (or key signal) of the SAW sensor. Therefore, this gas-sensitive layer, capable of efficiently and selectively adsorbing H_2S, are actually the key component of a SAW based H_2S gas sensors.

Previous studies revealed that metal oxides, such as CuO, ZnO, SnO_2, Fe_2O_3, WO_3,

have excellent adsorption ability toward H_2S [14-19]. Among them, CuO is usually used as the industrial desulfurizer, thus it could be a good candidate for the sensitive layer of the SAW H_2S gas sensor. Pristine CuO layers usually have a dense structure, which hinders the fast diffusion and release of H_2S molecules into or out from the sensitive layer. For example, our previous work reported a H_2S sensor based on sol-gel CuO films with a relative low porosity, and its response was not high (-8 kHz toward 2 ppm H_2S) [15]. Hence, it is necessary to develop highly porous CuO based sensitive layer to increase the sensitivity of the SAW sensor toward H_2S gas. In addition, as a desulfurizer, the adsorption capability of the CuO material toward H_2S is critically influenced by H_2O molecules in the air [20]. Therefore, when the CuO is used as the sensing layer of a SAW sensor, it is also critical to investigate the impact of humidity level on the sensing performance for H_2S. Nevertheless, very few studies focus on this critical problem and the mechanism is not well addressed.

To fabricating a highly porous CuO based sensitive film, we have utilized the sol-gel Al_2O_3 as the porous support to build a CuO-Al_2O_3 composite film in our previous work. However, the specific surface area and porosity of the film were less than 100 m^2/g and 10%, and the SAW sensor's response to 5 ppm H2S was less than -30 kHz [21]. Despite for the sol-gel method, electron beam evaporation (EBE) is another method, which can produce highly porous film. Especially for the amorphous Si film prepared by EBE, its porosity can be higher than 50%, which is superior than that prepared by sol-gel method [22,23]. In addition, the porous silicon is hydrophilic [24,25], which can effectively capture H_2O from the environment and are beneficial for the studying on the influence H_2O molecules on the

sensing performance. Therefore, in this work, by using the porous silicon as the support, we have constructed Si-Cu composites as the highly porous CuO based sensitive layers for SAW H_2S gas sensors by using the EBE method. Previous studies have revealed that CuO presents on the Cu content in the composite, which can serve as an adsorption site. Amorphous Si component in the layer produces a highly porous structure, which allows the uniform distribution of the Cu/CuO content and creates paths for effective gas diffusion/adsorption into the sensitive layer. Therefore, this Si-Cu composite layer shall be very sensitive toward H_2S and its sensing properties and mechanism are evaluated in this work. In addition, the influence of the humidity on the performance of the sensor was also investigated and the mechanism is discussed.

2.Experimental details

2.1 SAW Resonators

Two-port SAW resonators with a central frequency ~200 MHz, an insertion loss (*IL*) of -10.19 dB and a *Q* factor of 7529.2 were manufactured on ST-cut quartz substrates, as shown in Fig. 1. The detailed parameters of the resonator can be found in Supplementary Material.

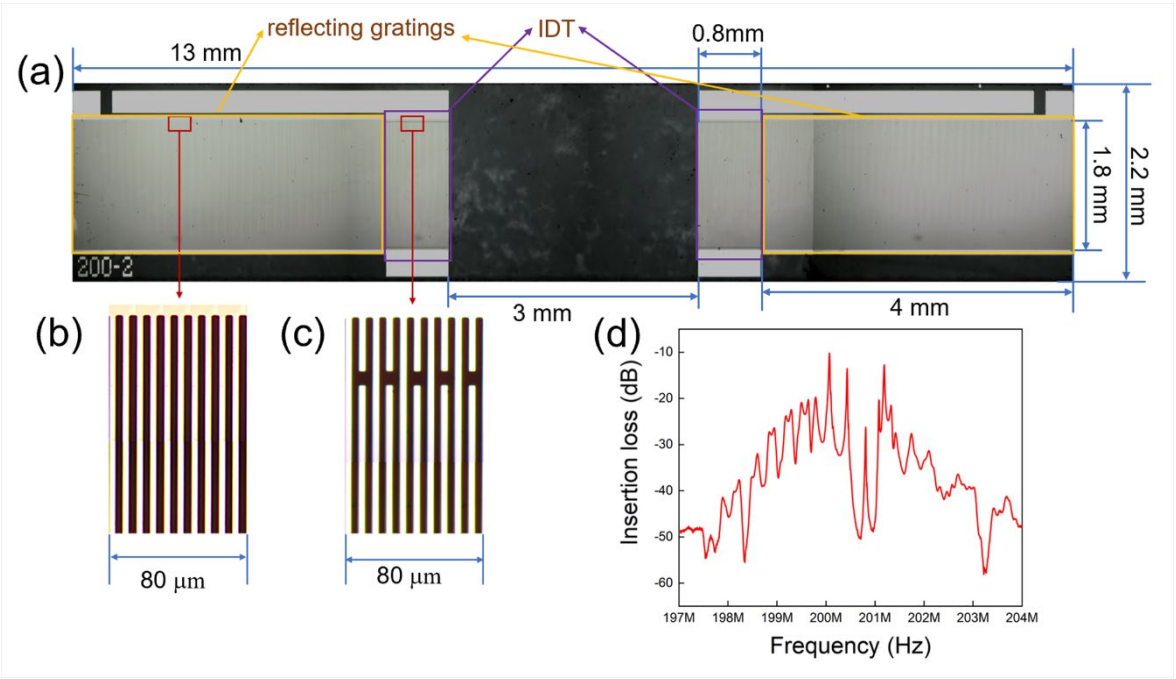

Fig. 1. (a) The optical microscopy image of a SAW resonator, (b) The reflecting gratings structure of the SAW resonator, (c) The IDTs structure of the SAW resonator, (d) The transmission feature (S_{21} parameter) of the SAW resonator

2.2 Sensitive layer preparation.

An electron beam evaporator, which has two electron guns to evaporate two different materials simultaneously, was used to deposited the Si-Cu layer. In our experiment, silicon and copper were co-evaporated onto the resonators at the same time to obtained Si-Cu composite layer. By adjusting the power of two electron guns, various evaporation rates of Si and Cu could be controlled, and four composite layers with different Si/Cu molar mass ratios (i.e., 1/0, 5.44/1, 3.09/1 and 2.08/1) were obtained. The thickness of each layer was

precisely controlled at 150 nm for all the samples by using a quartz crystal microbalance (QCM). For convenience, the layers with the Si/Cu ratios of 1/0, 5.44/1, 3.09/1 and 2.08/1 are denoted as S-1, S-2, S-3 and S-4, respectively. The coated resonators were then annealed at 200 ℃ for 2 hours in an air atmosphere to eliminate impurities in sensitive layers. The characterization methods for the Si-Cu layers can be found in the Supplementary Material.

2.3 Experimental setup and testing.

Peripheral circuits were connected to the coated resonators to construct SAW sensors (Fig. 2(a)). A homemade testing setup (Fig. 2(b)) were used to evaluate the sensing properties. The detailed gas sensing test procedure can be found in the Supplementary Material. For all the test procedures, the sensor was placed into the test chamber to interacting with the test gas for ~700 s. Sensor's response (Δf) equals the difference value between the sensor's oscillating frequency in the test gas (f_s) and that (f_0) in the fresh air, *i.e.*, $\Delta f = f_s - f_0$. After the test, the sensor was put into the fresh air to motivate the recovery.

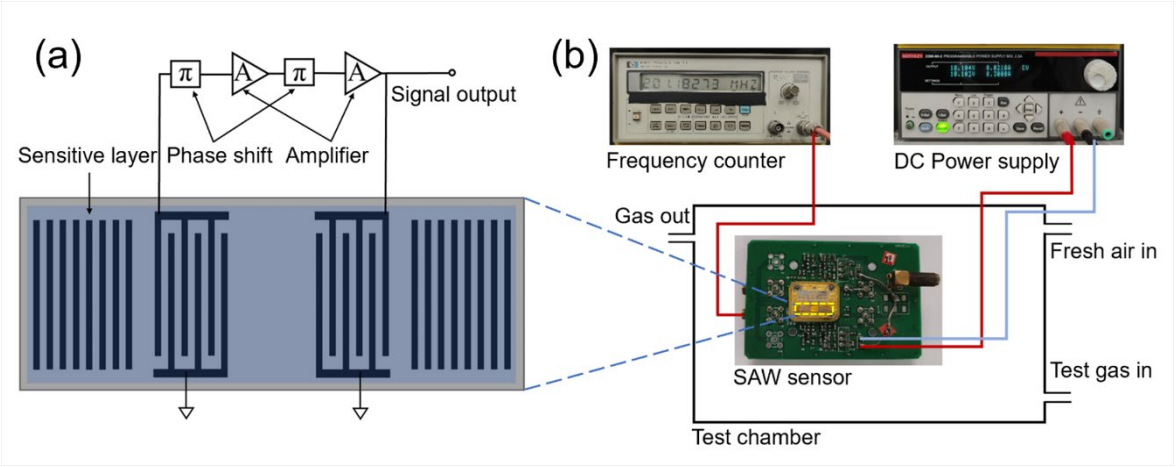

Fig. 2. (a) The senor's diagrammatic sketch; (b)the homemade testing setup

3. Results and Discussion

3.1 Characterization results.

Fig. 3 shows the Si and Si-Cu layers' scanning electron microscope (SEM) pictures. The Si layer (S-1) clearly exhibited a porous structure (Fig. 3(a)), with pore size around 24 nm. Figs. 3(b)-(d) show the surface morphologies of S-2, S-3 and S-4, and these Si-Cu composite layer' surfaces exhibit much denser nanoparticulate morphologies and less pores compared to those of pure Si layer. The pore volume is gradually decreased and the particle size remains 40 nm, as the Cu content ramps. The cross-sectional picture of the S-2 (The inset in Fig. 3(b)) shows the thickness of the layer is ~150.94 nm, which is in consistent with the value measured by the QCM.

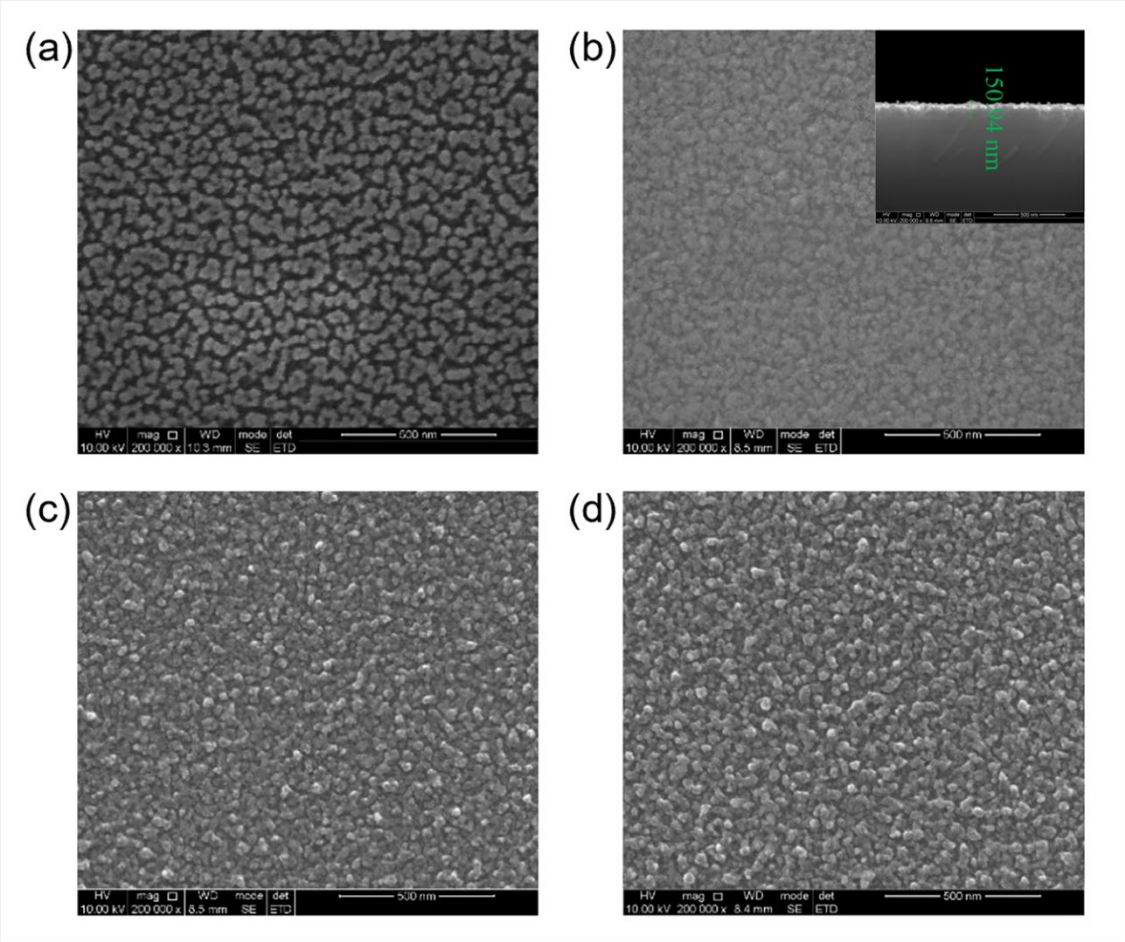

Fig. 3. SEM images of (a) S-1, (b) S-2, (c) S-3, (d) S-4. The inset in (c) shows the cross-sectional of the S-2

Si and Si-Cu composite layers' energy dispersive spectrometer (EDS) results (before and after they were tested with H_2S gas) are shown in Figs. 4(a)-(d). The inset images in Figs. 4(a)-(d) are enlarged view of the EDS results. As shown in Fig. 4(a), there is no Cu signal in the spectrum of the pristine Si layer (S-1). Whereas, Cu peaks can be found in Figs. 4(b)-(d) and its intensity enhances with the Cu ratio in the layer, indicating that the Cu atoms were successfully doped into the Si. By comparing the spectra of the layers before and after exposure to H_2S, it can be clearly found that S signal appears in the spectra of the composite layers after the exposure and the intensity of S signal increases with the increase of the Cu content. With these results, it can be concluded that Si can hardly adsorb H_2S molecules

while Cu plays as active sites for the H_2S adsorption and further reactions.

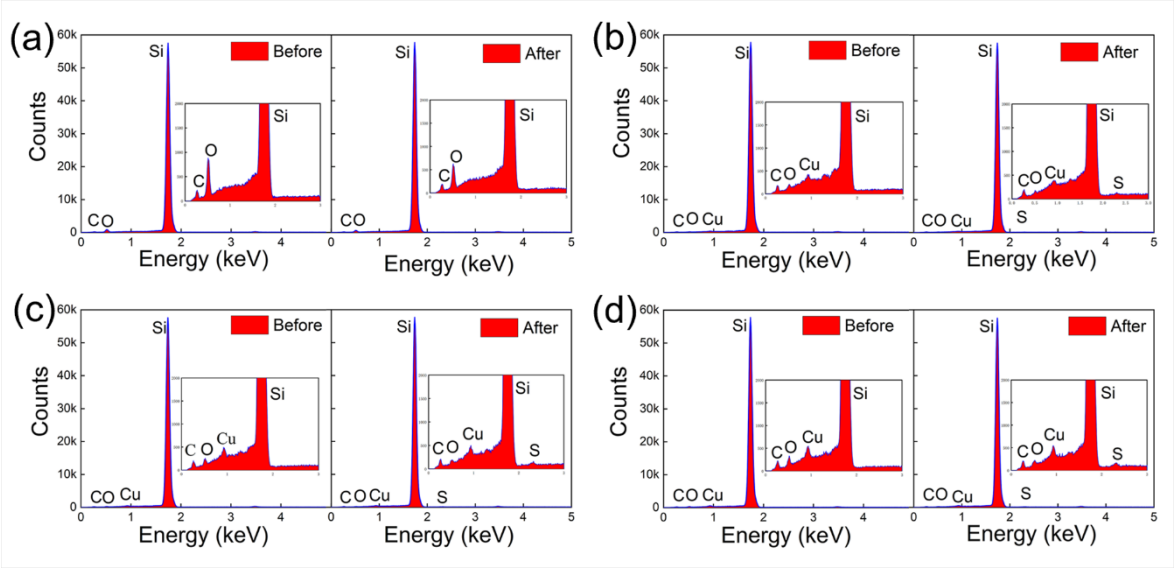

Fig. 4. EDS results of (a) S-1, (b) S-2, (c) S-3, (d) S-4 before and after exposure to H_2S gas

Raman spectra of the Si layer and the Si-Cu composite layers (before and after exposure to H_2S) are shown in Fig. 5(a). All the spectra have a peak centered at 518.3 cm^{-1}, which is related to Si. In addition, two bands located at 301 cm^{-1} and 618 cm^{-1} can be found in the spectrum of the Si-Cu layer before exposure to H_2S (Fig. 5b), which can be assigned as the Ag and B2g Raman modes of CuO, respectively [26-28]. This result indicates that CuO presents on the Cu in the composite. After the Si-Cu layer is exposed to H_2S, three peaks located at 471, 264 and 136 cm^{-1} appear (Fig 5a and c), which match well with the reported Raman spectra of CuS crystals [29-31]. Based on these Raman analysis results, the surface CuO, rather than Cu in the composite layer, truely adsorbs and chemically reacts with H_2S and then forms CuS.

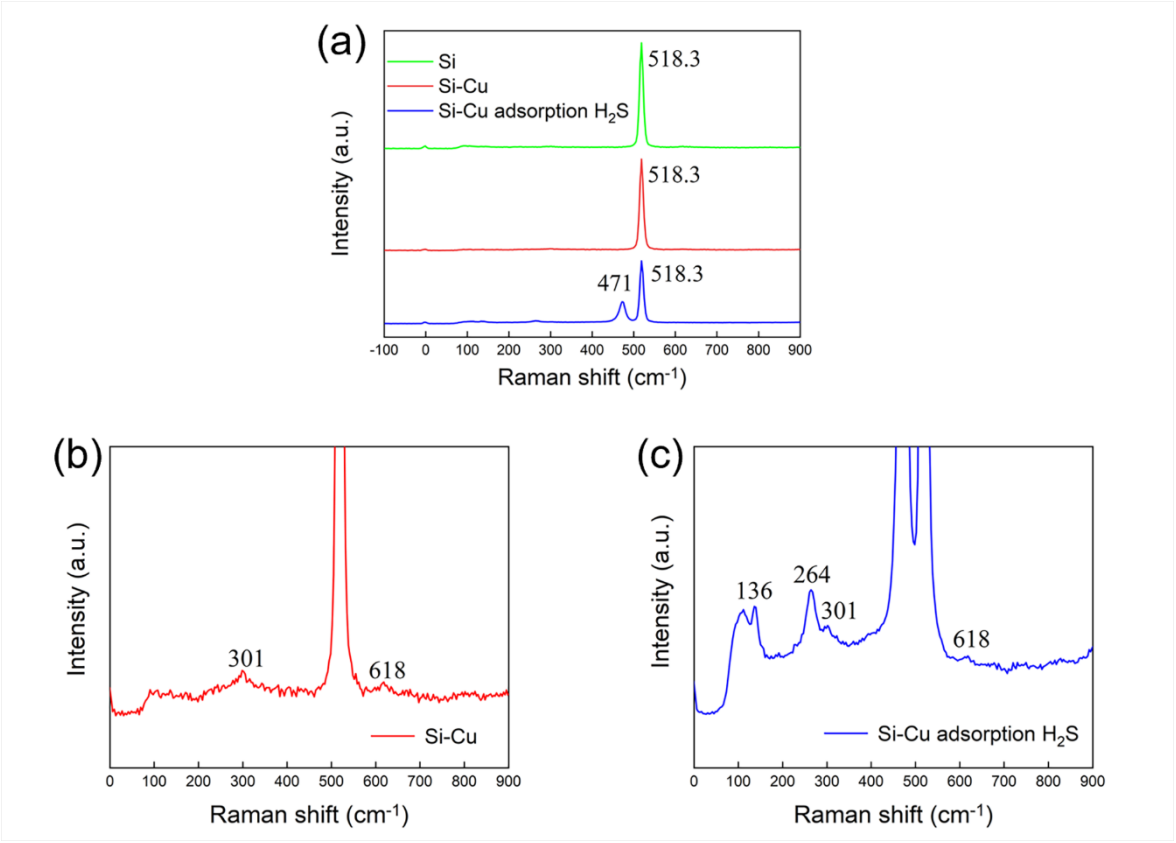

Fig. 5. Si layer and Si-Cu composite layers' Raman results

3.2 Sensor properties.

Frequency responses of the sensors toward 4 ppm H_2S at 25 °C and RH=60% are shown in Fig. 6(a). The Si layer based sensor responses only -4 kHz to the H_2S gas, whereas the sensors with the different Si-Cu composite layers show much stronger negative responses. In addition, the response enhances with the increase of the Cu content in the layer. For the sensors with S-2, S-3 and S-4 layers, their responses are -52 kHz, -109 kHz and -143 kHz, respectively. With this result, it can be concluded that the amount of Cu in composite plays a key factor for the sensitivity of the sensor because of the CuO on the Cu is an excellent adsorption site for H_2S, revealed by the EDS and Raman results. When the sensing process

is over, the sensors were exposed to fresh air to motivate the recovery. However, experimental results show that the recovery was sluggish at room temperature. To assist the recovery, the resonator was heated to ~200 °C for 2 minutes by using the Ni-Cr heater beneath the resonator, and then cooled down to 25 ℃. With this method, the full recovery of the sensors was achieved, and it could be also concluded that no more CuO was produced in the composite layers during the heat-treatment process.

Besides the response, the noise level and signal/noise ratio (SNR), which decides the sensitivity of the sensor, is the other key factor for a practical sensor. The noise level, defined as the maximum magnitude of the frequency jitter, of the sensors with S-2, S-3 and S-4 films are ~35, ~100 and ~260 Hz, respectively, as shown in fig.6(b). And the signal/noise ratio (SNR) are 1471, 1097, 550. The SNR decreases with the increase of the Cu content and the sensor with the S-2 layer has the highest SNR. Therefore, the sensor with the S-2 layer is selected for the subsequent experimental tests.

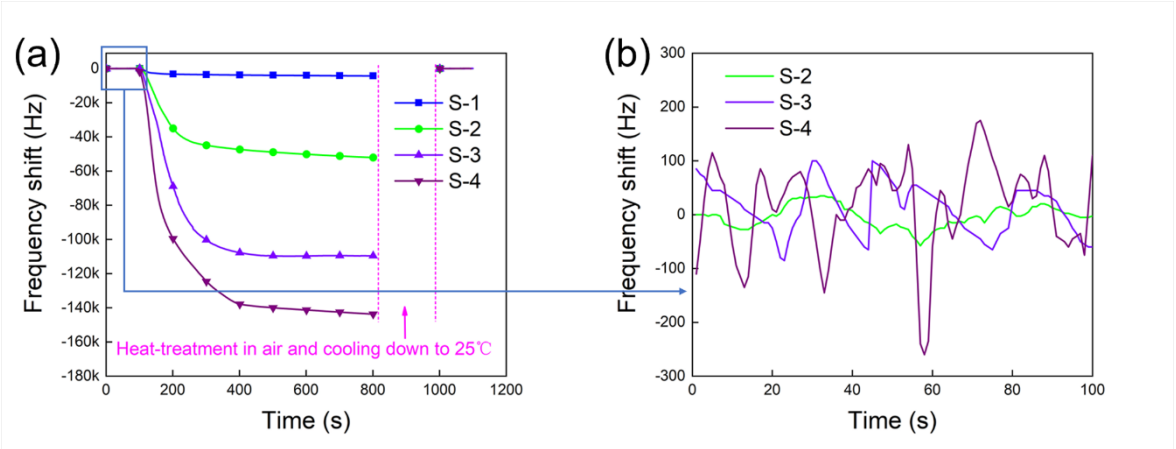

Fig. 6. (a) The response of the sensors with S-1, S2, S-3 and S-4 under 4 ppm H_2S; (b) the enlarged picture in the blue box in (a) showing the noise levels

Previous studies have revealed that the there is a significant humidity influence for a

SAW gas sensor [20]. Therefore, impact of the humidity on the sensor's response to H_2S were characterized under RH values of 50%, 60% and 70% at 25 ℃ (Fig. 7(a)). When the RH varies from 50% to 60% and 70%, the sensor's baseline negatively shifts −1.8 and −5.6 kHz, which indicate the Si-Cu layer can capture more H_2O in moister environment, resulting in the increase of the layer's mass or electrical conductivity. In addition, a significant increase in the sensor's response to 4 ppm H_2S can be also found in Fig. 7(a), when RH value increases from 50% to 70%. This result indicates that the H_2O molecules in the environment and on the sensitive layer may enhance the reaction between the H_2S and the sensitive layer.

Although the responses of the sensor become stronger at higher RH values, the noise level of the sensor also increases, and the signals of the sensor become unstable at RH=70% (Fig. 7(b)). In addition, when the RH value reaches 80%, the sensor stops oscillating. This is caused by the degradation of the insertion loss (*IL*) and *Q* factor of the SAW resonator induced by the more H_2O molecules adsorbed on the sensitive layer, which could absorb acoustic wave energy propagating through the SAW device (Figs. 7(c) and (d)). Therefore, for the following test, the RH is fixed at 60%.

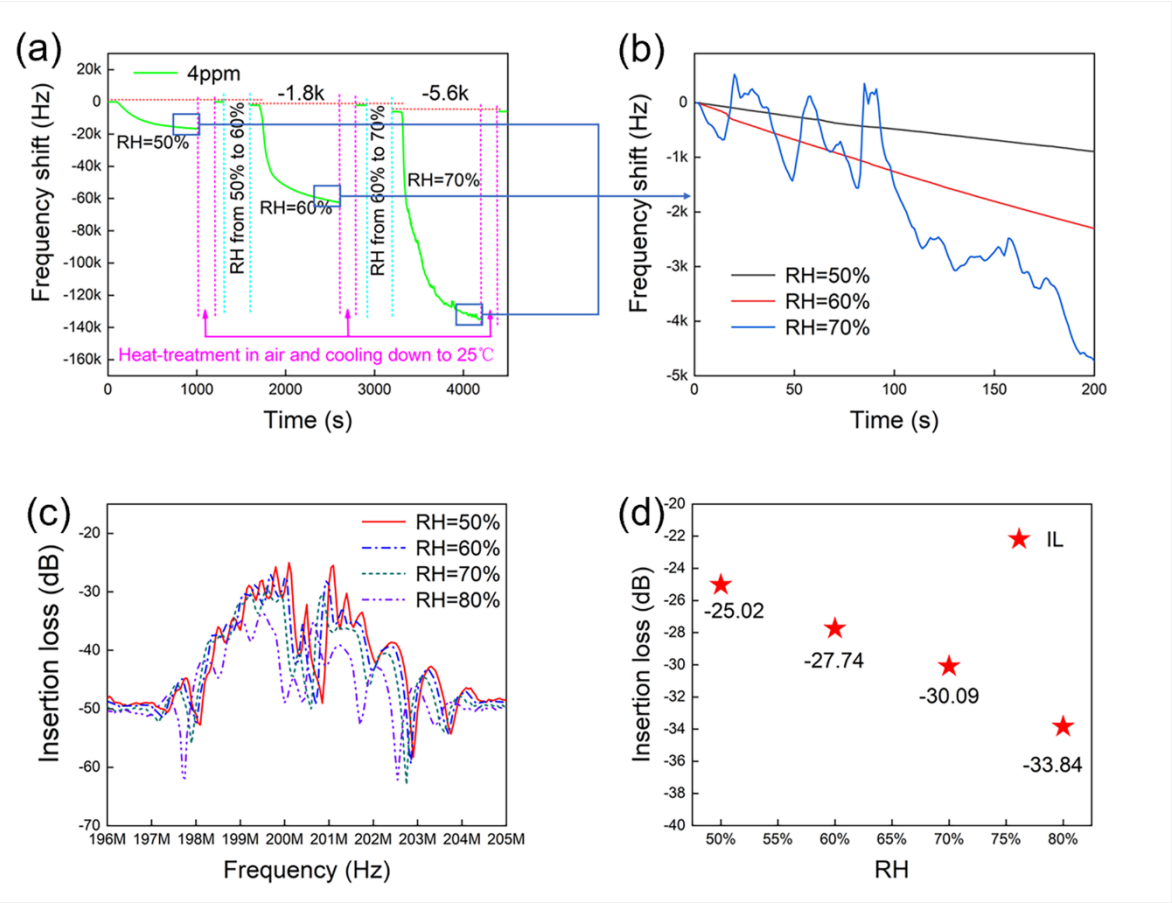

Fig. 7. (a) The responses of the sensor with S-2 to the RH and H_2S gas at different RH values; (b) The magnified pictures in the blue boxes in (a), indicating of noise levels of the sensor; The influence of RH on the (c) transmission feature and (d) insertion loss (*IL*) of the SAW resonator coated with the S-2

The sensor's dynamic responses to H_2S gas with various concentrations at 25 °C and RH=60% are presented in Fig. 8. As is shown, the response increases from -0.2 kHz to -122 kHz when the concentration varies from 50 ppb to 16 ppm. After each response process (each process was kept at ~700 s), the sensor is exposed to fresh air and the resonator is heated to 200 °C for 2 minutes then cooled at room temperature to achieve the recovery.

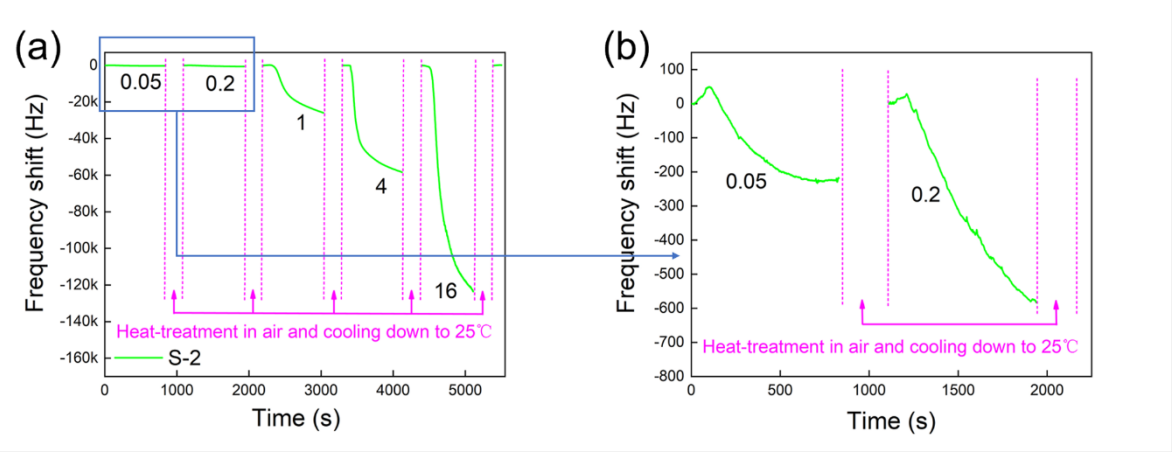

Fig. 8. (a) Dynamic responses of the Sensor with the S-2 to 0.05−16 ppm H_2S gas; (b) the magnification of the blue box in (a)

The sensor's reproducibility was examined by putting it into a H_2S environment (4 ppm) for three successive cycles. The sensor exhibits the similar response in these three cycles, and the frequency shifts are ~-55 kHz, demonstrating the good stability (Fig. 9(a)). The sensor's selectivity was also investigated by putting it in environments with hydrogen, carbon monoxide, methane, nitrogen dioxide, ethanol, ammonia and hydrogen sulfide, respectively, at RH=60% and 25 °C. A negative frequency shift of -14 kHz can be observed when the sensor is in 100 ppm ammonia (Fig. 9(b)), whereas there are no responses towards other gases. The response toward ammonia may be caused by the ammonia molecules absorbed by the water in the sensor layer [32,33]. However, the response of the sensor to 100 ppm NH_3 (~ -14 kHz) is much weaker than that to 4 ppm H_2S (~ -55 kHz), indicating that the sensor has an excellent selectivity to H_2S. The long-term stability of the sensor was further studied by conducting sensing tests every 5 days in a 20-day period (Fig. 9(c)), the result shows that the sensor's response fluctuated less than 20%, indicating the good long-term stability.

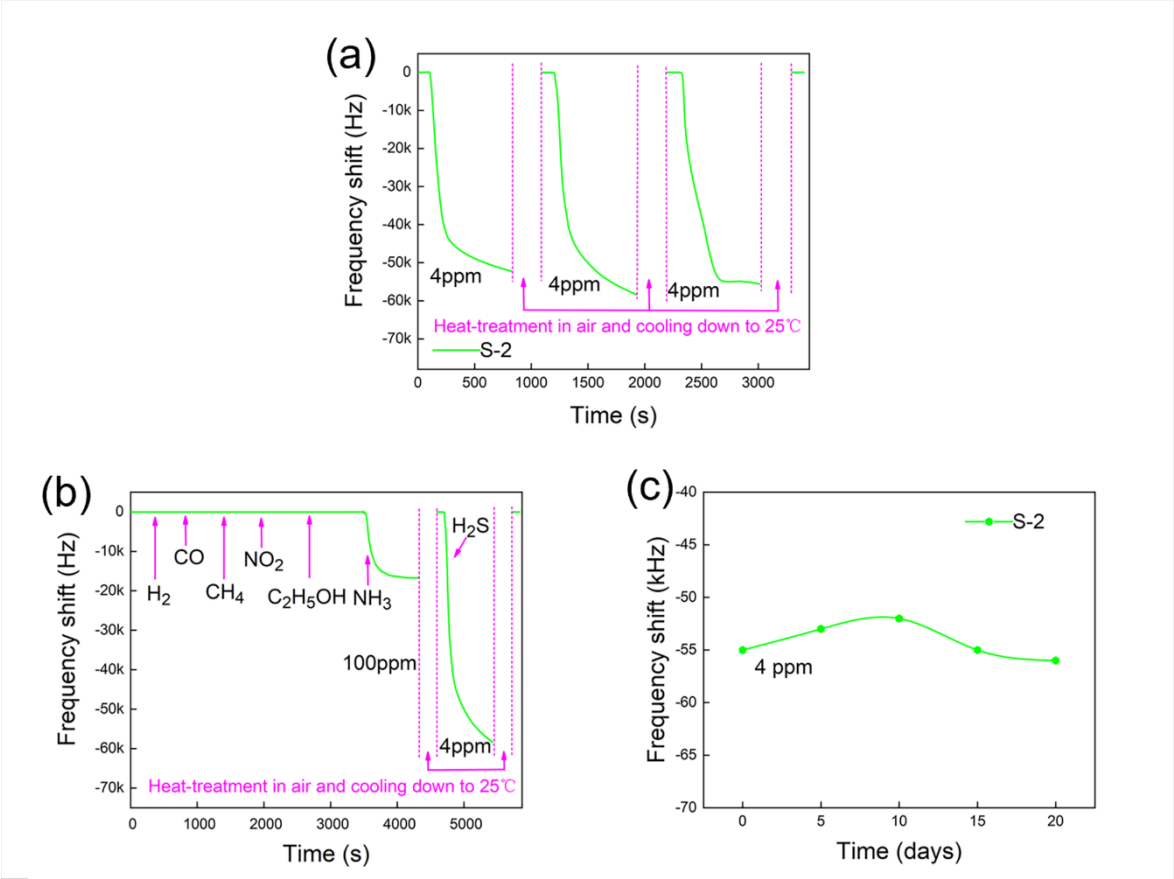

Fig. 9. (a) The sensor's response to H_2S at RH = 60% and 25 °C for 3 successive cycles; (b) Responses of the sensor to 100 ppm hydrogen, carbon monoxide, methane, nitrogen dioxide, ethanol, ammonia and 4 ppm hydrogen sulfide; (c) The long-term stability

3.3 Sensing mechanism.

Variations on the sensing layers' mass, elastic modulus and electrical conductivity are accountable for SAW sensor' responses [16,34]. These three variations can be denoted as mass, elastic and electrical loading effects, and can affect the sensor's working frequency (f) and response (Δf) in the way shown in Table S1 [16].

The influence of electrical loading effect was firstly evaluated. The sheet conductivity (σ_s) of the S-2 on the SAW resonator was increased from 3.15×10^{-13} S/m to 1.02×10^{-12} S/m when it was exposed to 4 ppm H_2S gas at room temperature for the first time (Fig. 10). The

recovery of σ_s value cannot be achieved after the exposure neither, whereas it happens after the heating process, which is in accordance with the frequency measurement.

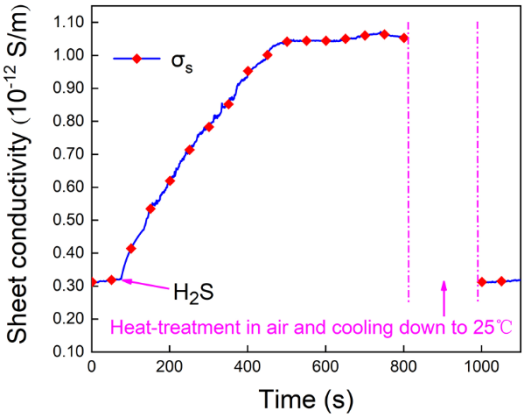

Fig. 10. S-2 layer's dynamic sheet conductivity when it is in 4 ppm H_2S

The electric loading affects the frequency response (Δf) as following [34],

$$\Delta f = -f_0 \times \frac{K^2}{2} \times \Delta\left(\frac{1}{1+\left(\frac{v_0 C_s}{\sigma_s}\right)^2}\right) \quad (1)$$

where v_0 (=3158 m/s), f_0 (=~201 MHz), C_s (= ~5.0×10^{-11} F/m), K^2 (= 0.0011) are the unperturbed SAW velocity, resonant frequency, capacitance per unit length and electromechanical coupling coefficient of the ST-cut quartz SAW resonator, respectively. By using the equation (1) and the measured σ_s, the calculated Δf induced by the electrical loading effect is -4.8×10^{-6} Hz, which is neglectable compared with the measured responses. Hence, the measured responses must be caused by other factors, e.g., mass loading or elastic loading effects.

EDS and Raman characterization results have revealed that the CuO in the sensitive layer can react with H_2S when the sensitive layer is exposed to H_2S, and the reaction formula

can be expressed as [17]:

$$CuO + H_2S(ads) = CuS + H_2O \quad (2)$$

After the reaction, formation of CuS with a higher molar mass than that of CuO on the surfaces, results in an increase in the mass of the sensitive layer. This causes a negative frequency shift of the sensor, as shown in Table S1. Besides, formation of CuS also leads to an increase of the elastic moduli of the sensitive layer as discussed in our previous work [35] which results in a positive frequency response of the sensor (Table S1). Nevertheless, all the measured frequency shifts of our sensors are negative, which indicates that the mass loading effect dominates frequency response.

The reaction between CuO and H_2S (equation (2)) is irreversible and exothermic at room temperature because of the negative enthalpy of the reaction [17,36], which is accountable for the sensor's sluggish recovery. However, it have been proved the high temperature (>200 ^oC) may enable the inverse reaction [17,36]. As a result, a heat-treatment process can accelerate the sensor's recovery (Figs. 6-10).

Previous studies have revealed that the reaction (2) can be significantly affected by the adsorbed H_2O molecules on the CuO's surface [20]. H_2O molecules adsorbed on the CuO surface are condensed and a H_2O layer is formed, both of which result in the formation of Cu^{2+} and OH^-. When exposed to H_2S, H_2S molecules dissolve in the H_2O layer and react with OH^- and the reaction product is HS^-/S^{2-}. HS^-/S^{2-} will finally react with Cu^{2+}, leading to the formation of CuS, as shown in Fig. 11. The whole above reaction process can be expressed as follows [20]:

$$CuO + H_2O \rightleftharpoons Cu^{2+} + 2OH^- \quad (3)$$

$$H_2S + H_2O \rightleftharpoons HS^- + H_3O^+ \quad (4)$$

$$H_2S + OH^- \rightleftharpoons HS^- + H_2O \quad (5)$$

$$HS^- + OH^- \rightleftharpoons S^{2-} + H_2O \quad (6)$$

$$Cu^{2+} + S^{2-} \rightleftharpoons CuS \quad (7)$$

This reaction process clearly indicates that the presence of H_2O in the environment will enhance the reaction between CuO and H_2S, therefore the response of the sensor is much stronger in the environment with higher RH values (e.g., 60%) as is shown in Fig. 7(a).

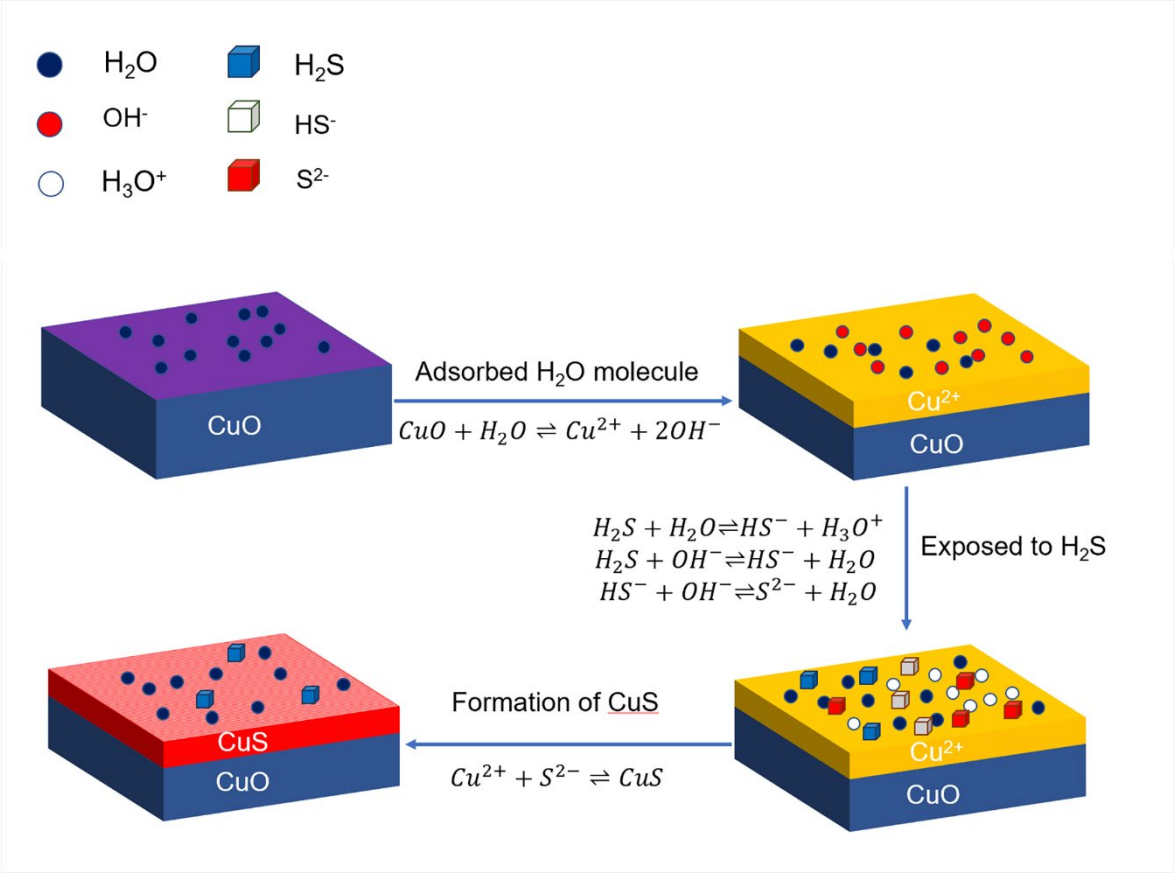

Fig. 11. The schematic of H_2S molecules diffusing on the surface of layer and into the layer

4. Conclusions

Sensing performance and mechanism of surface acoustic wave (SAW) H_2S gas sensors based on electron beam evaporation Si-Cu composite layer were investigated. The Si content leads to a porous structure of the layer beneficial for the interaction between the layer and H_2S. The CuO content in the composite layer plays a key role for H_2S response of the sensor since it can act as the active sites for the adsorption and reaction of H_2S. The reaction between CuO and H_2S results in the formation of the CuS, causing an increase in the mass of the composite layer and leading to the negative frequency response of the SAW sensor. The humidity is highly influential on the sensing performance of the sensor because the H_2O molecules participate the reactions between CuO and H_2S. With higher RH values, the sensor exhibits much stronger responses but higher noise level because more H_2O on the layer leads to a higher insertion loss and lower Q factor of the SAW device.

Acknowledgments

This work was supported by the Natural Science Foundation of Sichuan province (2022NSFSC1981), National Natural Science Foundation of China (61178018), and the Engineering Physics and Science Research Council of UK (EP/P018998/1) and International Exchange Grant (201078) through Royal Society and NFSC.

Conflicts of interests

The authors declare no competing financial interest.

References

[1] T.L. Guidotti, Hydrogen sulfide intoxication, Handbook of clinical neurology. Vol. 131. Elsevier (2015) 111-133. https://doi.org/10.1016/B978-0-444-62627-1.00008-1.

[2] T.S. Carpenter, S.M. Rosolina, Z.L. Xue, Quantitative, colorimetric paper probe for hydrogen sulfide gas, Sens. Actuators B Chem. 253 (2017) 846-851. https://doi.org/10.1016/j.snb.2017.06.114.

[3] P. Haouzi, T. Sonobe, A. Judenherc-Haouzi, Developing effective countermeasures against acute hydrogen sulfide intoxication: challenges and limitations, Ann. N. Y. Acad. Sci. 1374 (2016) 29-40. https://doi.org/10.1111/nyas.13015.

[4] W. Rumbeiha, E. Whitley, P. Anantharam, D.S. Kim, A. Kanthasamy, Acute hydrogen sulfide–induced neuropathology and neurological sequelae: challenges for translational neuroprotective research, Ann. N. Y. Acad. Sci. 1378 (2016) 5-16. https://doi.org/10.1111/nyas.13148.

[5] A. El Brahmi, S. Abderafi, Hydrogen sulfide removal from wastewater using hydrogen peroxide in-situ treatment: Case study of Moroccan urban sewers, Mater. Today Proceedings 45 (2021) 7424-7427. https://doi.org/10.1016/j.matpr.2021.01.641.

[6] K.I. Adeniyi, H.H. Wan, C.E. Deering, F. Bernard, M.A. Chisholm, R.A. Marriott, High-pressure hydrogen sulfide experiments: how did our safety measures and hazard control work during a failure event? Safety 6 (2020) 15. https://doi.org/10.3390/safety6010015.

[7] I.M. Nassar, M.N. El-Din, R.E. Morsi, A. Abd El-Azeim, A.I. Hashem, Eco Friendly nanocomposite materials to scavenge hazard gas H_2S through fixed-bed reactor in petroleum

application, Renew. Sust. Energ. Rev. 65 (2016) 101-112. https://doi.org/10.1016/j.rser.2016.06.019.

[8] M.M. Asad, R.B. Hassan, F. Sherwani, Q.M. Soomro, S. Sohu, M.T. Lakhiar, Oil and gas disasters and industrial hazards associated with drilling operation: an extensive literature review, 2019 2nd International Conference on Computing, Mathematics and Engineering Technologies (iCoMET). IEEE, 2019. 10.1109/ICOMET.2019.8673516.

[9] K.H. Kim, E.C. Jeon, Y.J. Choi, Y.S. Koo, The emission characteristics and the related malodor intensities of gaseous reduced sulfur compounds (RSC) in a large industrial complex, Atmos. Environ. 40 (2006) 4478-4490. https://doi.org/10.1016/j.atmosenv.2006.04.026.

[10] W.A.N.G. Qian, Generation mechanism and control measures for H_2S in oil wells, Liaohe Oilfield, Petrol. Explor. Dev. 35 (2008) 349-354. https://doi.org/10.1016/S1876-3804(08)60082-8.

[11] C.H. Gammons, S.R. Poulson, J.J. Metesh, T.E. Duaime, A.R. Henne, Geochemistry and isotopic composition of H_2S-rich water in flooded underground mine workings, Butte, Montana, USA, Mine Water Environ. 22 (2003) 141-148. https://doi.org/10.1007/s10230-003-0014-y.

[12] X. Liu, W. Wang, Y. Zhang, Y. Pan, Y. Liang, J. Li, Enhanced sensitivity of a hydrogen sulfide sensor based on surface acoustic waves at room temperature, Sensors 18 (2018) 3796. https://doi.org/10.3390/s18113796.

[13] M. Asad, M.H. Sheikhi, Surface acoustic wave based H_2S gas sensors incorporating sensitive layers of single wall carbon nanotubes decorated with Cu nanoparticles, Sens. Actuators B Chem. 198 (2014) 134–141. https://doi.org/10.1016/j.snb.2014.03.024.

[14] W. Luo, J. Deng, Q. Fu, D. Zhou, Y. Hu, S. Gong, Z. Zheng, Nanocrystalline SnO_2 layer prepared by the aqueous sol–gel method and its application as sensing layers of the resistance and SAW H_2S sensor, Sens. Actuators B Chem. 217 (2015) 119–128. https://doi.org/10.1016/j.snb.2014.10.078.

[15] D.J. Li, X.T. Zu, D.Y. Ao, Q.B. Tang, Y.Q. Fu, Y.J. Guo, High humidity enhanced surface acoustic wave (SAW) H_2S sensors based on sol–gel CuO films, Sens. Actuators B Chem. 294 (2019) 55-61. https://doi.org/10.1016/j.snb.2019.04.010.

[16] Y.L. Tang, X.F. Xu, S.B. Han, C. Cai, H.R. Du, H. Zhu, X.T. Zu, Y.Q. Fu, ZnO-Al_2O_3 nanocomposite as a sensitive layer for high performance surface acoustic wave H_2S gas sensor with enhanced elastic loading effect, Sens. Actuators B Chem. 304 (2020) 127395. https://doi.org/10.1016/j.snb.2019.127395.

[17] N.S. Ramgir, C.P. Goyal, P.K. Sharma, U.K. Goutam, S. Bhattacharya, N. Datta, S. K. Gupta, Selective H_2S sensing characteristics of CuO modified WO_3 thin films, Sens. Actuators B Chem. 188(2013) 525-532. https://doi.org/10.1016/j.snb.2013.07.052.

[18] Z.L. Wu, Z.J. Li, H. Li, M.X. Sun, S.B. Han, C. Cai, W.Z. Shen, Y.Q. Fu, Ultrafast response/recovery and high selectivity of the H_2S gas sensor based on α-Fe_2O_3 nano-ellipsoids from one-step hydrothermal synthesis, ACS Appl. Mater. Inter. 11 (2019) 12761-12769. https://doi.org/10.1021/acsami.8b22517.

[19] T.T.N. Hoa, D.T.T. Le, N. Van Toan, N. Van Duy, C.M. Hung, N.V. Hieu, N.D. Hoa, Highly selective H_2S gas sensor based on WO_3-coated SnO_2 nanowires, Mater. Today Commun. 26 (2021) 102094. https://doi.org/10.1016/j.mtcomm.2021.102094.

[20] J. Wang, L.J. Wang, H.L. Fan, H. Wang, Y.F. Hu, Z.D. Wang, Highly porous copper oxide sorbent for H_2S capture at ambient temperature, Fuel 209 (2017) 329-338. https://doi.org/10.1016/j.fuel.2017.08.003.

[21] Y.L. Tang, W. Wu, B.J. Wang, X.C. Dai, W.F. Xie, Y.W. Yang, R.J. Zhang, X. Xiang, X.T. Zu, Y.Q. Fu, H_2S gas sensing performance and mechanisms using CuO-Al_2O_3 composite films based on both surface acoustic wave and chemiresistor techniques, Sens. Actuators B Chem. 325 (2020) 128742. https://doi.org/10.1016/j.snb.2020.128742.

[22] K. Kaminska, T. Brown, G. Beydaghyan, K. Robbie, Vacuum evaporated porous silicon photonic interference filters, Appl. optics 42 (2003) 4212-4219. https://doi.org/10.1364/AO.42.004212.

[23] M. Riley, A. Redo-Sanchez, P. Karampourniotis, J. Plawsky, T.M. Lu, Nanostructured porous silicon films for terahertz optics, Nanotechnology 23 (2012) 325301. DOI 10.1088/0957-4484/23/32/325301.

[24] C.Y. Chang, C.Y. Lin, D.S. Lin, How dissociated fragments of multiatomic molecules saturate all active surface sites—H_2O adsorption on the Si (100) surface, J. Phys. Condens. Mat. 33 (2021) 404004. DOI 10.1088/1361-648X/ac14f7.

[25] D. Schmeisser, A comparative study of O_2, H_2 and H_2O adsorption on Si (100), Surf. Sci. 137 (1984) 197-210. https://doi.org/10.1016/0039-6028(84)90685-X.

[26] T.H. Tran, V.T. Nguyen, Phase transition of Cu_2O to CuO nanocrystals by selective laser heating, Mat. Sci. Semicon. Proc. 46 (2016) 6-9. https://doi.org/10.1016/j.mssp.2016.01.021.

[27] P.V. Tong, N.D. Hoa, H.T. Nha, N.V. Duy, C.M. Hung, N.V. Hieu, SO_2 and H_2S sensing properties of hydrothermally synthesized CuO nanoplates, J. Electron. Mater. 47 (2018) 7170-7178. https://doi.org/10.1007/s11664-018-6648-0.

[28] C.H. Tsai, P.H. Fei, C.M. Lin, S.L. Shiu, CuO and CuO/graphene nanostructured thin films as counter electrodes for Pt-free dye-sensitized solar cells, Coatings 8 (2018) 21. https://doi.org/10.3390/coatings8010021.

[29] T. Hurma, S. Kose, XRD Raman analysis and optical properties of CuS nanostructured film, Optik 127 (2016) 6000-6006. https://doi.org/10.1016/j.ijleo.2016.04.019.

[30] Y.Q. Zou, L. Jiang, T.F. Zhai, T.T. You, X.F. Jing, R.Y. Liu, F.H. Li, W. Zhou, S.Z. Jin, Surface-enhanced Raman scattering by hierarchical CuS microflowers: Charge transfer and electromagnetic enhancement, J. Alloys. Compd. 865 (2021) 158919. https://doi.org/10.1016/j.jallcom.2021.158919.

[31] Y. Qin, X.G. Kong, D.Q. Lei, X.D. Lei, Facial grinding method for synthesis of high-purity CuS nanosheets, Ind. Eng. Chem. Res. 57 (2018) 2759-2764. https://doi.org/10.1021/acs.iecr.7b04616.

[32] M. Sodupe, A. Oliva, J. Bertran, Theoretical study of the ionization of the H_2O-H_2O, NH_3-H_2O, and FH-H_2O hydrogen-bonded molecules, J. Am. Chem. Soc. 116 (1994) 8249-8258.

[33] J.E. Bertie, M.M. Morrison, The infrared spectra of the hydrates of ammonia, $NH_3 \cdot H_2O$

and $2NH_3 \cdot H_2O$ at 95° K, J. Chem. Phys. 73 (1980) 4832-4837. https://doi.org/10.1063/1.440002.

[34] A.J. Ricco, S.J. Martin, T.E. Zipperian, Surface acoustic wave gas sensor based on film conductivity changes, Sens. Actuators 8 (1985) 319–333. https://doi.org/10.1016/0250-6874(85)80031-7.

[35] S. Arora, K. Kabra, K.B. Joshi, B.K. Sharma, G. Sharma, Structural, elastic, thermodynamic and electronic properties of covellite, CuS, Physica B 582 (2020) 311142. https://doi.org/10.1016/j.physb.2018.11.007.

[36] N.S. Ramgir, S. Kailasa Ganapathi, M. Kaur, N. Datta, K.P. Muthe, D.K. Aswal, S.K. Gupta, J.V. Yakhmi, Sub-ppm H_2S sensing at room temperature using CuO thin films, Sens. Actuators B Chem. 151 (2010) 90-96. https://doi.org/10.1016/j.snb.2010.09.043.